

The symbiotic system AG Draconis

Soft X-ray bremsstrahlung from the nebulae

Marcella Contini¹ and Rodolfo Angeloni²

¹*School of Physics and Astronomy, Tel-Aviv University, Tel-Aviv, 69978 Israel*

²*Departamento de Astronomía y Astrofísica, Pontificia Universidad Católica de Chile - Vicuña Mackenna 4860, 7820436 Macul, Santiago, Chile*

Abstract

The modeling of UV and optical spectra emitted from the symbiotic system AG Draconis, adopting collision of the winds, predicts soft X-ray bremsstrahlung from nebulae downstream of the reverse shock with velocities $> 150 \text{ km s}^{-1}$ and intensities comparable to those of the white dwarf black body flux. At outbursts, the envelop of debris, which corresponds to the nebula downstream of the high velocity shocks ($700\text{-}1000 \text{ km s}^{-1}$) accompanying the blast wave, absorbs the black body soft X-ray flux from the white dwarf, explains the broad component of the H and He lines, and leads to low optical-UV-X-ray continuum fluxes. The high optical-UV flux observed at the outbursts is explained by bremsstrahlung downstream of the reverse shock between the stars. The depletion of C, N, O, and Mg relative to H indicates that they are trapped into dust grains and/or into diatomic molecules, suggesting that the collision of the wind from the white dwarf with the dusty shells, ejected from the red giant with a ~ 1 year periodicity, leads to the U-band fluctuations during the major bursts.

Keywords: binaries: symbiotic - stars: individual: AG Dra

1. Introduction

Circumstellar and circumbinary nebulae throughout symbiotic systems (SS) emit line spectra and continuum in the radio, infrared (IR), optical, UV, and X-ray range (Angeloni et al. 2010 and references therein).

The two main SS components, generally a white dwarf (WD) and a red giant (RG) rotating in bound orbits, lead to characteristic time periodicities. Moreover, they dominate the continuum spectral energy distribution (SED) in the UV-soft X-rays and IR-optical ranges, respectively.

The RG flux is well reproduced by a black body (bb). The analysis of symbiotic systems shows that the flux from the hot component star is approximated by a bb which peaks in the far UV. It was rarely observed, beyond a few data in the bb low frequency tail. Consequently, the temperature of the hot star was obtained indirectly from the characteristic spectral line ratios emitted from the nebulae (Angeloni et al. 2010).

AG Draconis (AG Dra) is classified as a yellow symbiotic binary containing a K2III giant (Mürset & Schmid 1999) and a WD accreting from the giant's wind on a 549 day orbit (Fekel et al. 2000). The orbital inclination is relatively low with $i \sim 30^\circ\text{-}45^\circ$ (Mikolajewska et al. 1995) or $i \sim 60 \pm 8.2^\circ$ (Schmid & Schild 1997). In fact, during the orbital motion the WD is not eclipsed.

The light curve of AG Dra shows numerous bursts with amplitude spanning 1-3 mag in U. González-Riestra et al. (1999, hereafter GVIG99) identified "cool" and "hot" outbursts differing in Zanstra temperature and light curve profile (Skopal et al. 2009). Tomov & Tomova (2002 and references therein) report from the analysis of the photometric data that the visual light

growth during the optical brightening is due to increased radiation of the circumbinary nebula. Thermonuclear events on the surface of the WD (Mikolajewska et al. 1995) and expansion and cooling of the compact secondary (Greiner et al. 1997) were also conjectured to explain the outbursts.

Besides the characteristic outbursts in the U band, AG Dra is the brightest system at soft X-ray energies of all SS. Viotti et al. (1998) monitored the super soft X-rays from the AG Dra source by EXOSAT and ROSAT and the UV flux by IUE. It was found that during all the monitored outbursts the visual magnitude was associated with an increase in the UV flux, while the X-ray count rate largely faded, namely the count rate dramatically dropped at the time of the 1985 and 1986 maxima (Viotti et al. 1998) and between 1992 and 1996 (Greiner et al. 1997). Actually, Viotti et al. (1998) discovered the systematic optical/UV and X-ray flux anti-correlation, which was confirmed by Skopal et al. (2009), González-Riestra et al. (2008), etc. observations.

Analyzing new data by XMM Newton and FUSE, Skopal et al. (2009) recently concluded that the soft X-ray emission is produced by the WD photosphere. They claim that X-ray and far UV observations determine the bb temperature unambiguously. Modeling the UV and super-soft X-ray data in AG Dra, they concluded that the observed anti-correlation is caused by the variable wind from the hot star, explaining that the enhanced hot star wind gives rise to the optical bursts by reprocessing high energy photons from the Lyman continuum to the optical/UV.

This paper is motivated by the analysis of AG Dra XMM-Newton observations (Jansen et al. 2001) performed during the

2003 hot burst and during quiescent phases by Skopal et al. (2009), who found that the soft X-ray spectrum at quiescence corresponds to bb radiation. We would like to investigate by consistent modeling of the line and continuum spectra whether the bremsstrahlung downstream of shocked nebulae might contribute to the soft X-ray emission at different phases.

Significant information about the physical conditions of the SS components can be obtained by line spectrum analysis. The intensities and profiles of some spectral lines emitted from AG Dra at different epochs were analyzed in detail (e.g. the $H\alpha$ and $HeII$ 4713 lines by Tomov & Tomova 2002, the OVI 1032, 1035 doublet and $HeII$ 1640 line by Skopal et al. 2009). The most comprehensive and complete sample of spectra in number of lines at different close phases in the optical and UV ranges was provided by GVIG99. Both the line and continuum spectra were explained by photoionization of circumstellar matter, e.g. the wind from the RG, and of circumbinary matter by the hot star radiation flux.

Viotti et al. (1989) noticed, however, that *in some models X-ray are interpreted as bremsstrahlung emission from the collision of the winds from both components (e.g. Kwok & Leahy 1984, Girard & Willson 1987). The steady and intense X-ray emission of AG Dra during quiescence indicates the presence of an effective heating process.*

Therefore in this paper we calculate the spectra using composite models which account consistently for shocks and photoionization. We will follow the method adopted by Angeloni et al. (2010) for other symbiotic systems, cross-checking the calculations of the continuum by those of the line ratios. We will focus on the optical-UV-X-ray domain, leaving the radio-IR range to the next investigation of the AG Dra SS.

The models presented by Skopal et al. (2009) for AG Dra are valid on a large scale, namely the continuum emitted from the nebulae was not constrained by the analysis of the line spectra. The collision of the winds cannot be neglected because it leads to high temperatures of the gas. In this paper we would like therefore to investigate whether, adopting models accounting for both photoionization and shocks, it is possible to add some information to the interpretation of AG Dra spectral features, in particular, and of SSs, in general.

The SS modeling and the calculation of the spectra are explained in Sect. 2. The spectra are analyzed in Sect. 3. Results are presented in Sect. 4. Discussion and concluding remarks follow in Sect. 5.

2. The models

Alternating episodes of accretion and wind collision were evident during the evolution of symbiotic systems, e.g. CH Cyg. The epochs treated in this work on AG Dra are close to outbursts. We consider that the accretion disk was blown up and had no time to form. In fact, the observed spectra do not show the typical double peaked lines. So we adopt the colliding wind model of Girard & Willson (1987), which applies close to the orbital plane of the SS.

2.1. Wind collision theory

Girard & Willson (1987) explained that in a widely separated binary consisting of a late giant and a hot WD, the late star has a stellar wind with a mass loss rate of 10^{-7} - $10^{-5} M_{\odot} \text{ yr}^{-1}$ and a velocity ~ 10 - 30 km s^{-1} . The hot star will accrete hydrogen rich material from the late red giant wind. Theoretical models by Paczynski & Zytlow (1978) show that an accretion of hydrogen rich material at a rate of 10^{-11} to $10^{-10} M_{\odot} \text{ yr}^{-1}$ will generate periodic hydrogen shell flashes, with each outburst lasting on the order of decades. The increased flux from such an eruption, particularly in the UV region, and the accompanying increase in radiation pressure will tend to eject the hot star's hydrogen atmosphere in the form of a stellar wind with velocities of 1000-3000 km s^{-1} (Conti 1978), which may last for decades. Both the winds from the WD and the red giant are supersonic, so shocks will form.

Since the end of the 1990, it was suggested by the analysis of SS line spectra (Nussbaumer 2000 and references therein) that both stars lose winds which collide in the interbinary region and outward, creating a network of shock-fronts. A picture of the colliding wind model adapted to the presence of dust shells is given by Contini et al. (2009c, fig. 2).

The scenario shows the collision of the winds from both stars leading to two shock-fronts which propagate between the stars: the strong one, dominating the spectrum, propagates in reverse towards the WD, and the weaker one, not always important, propagates towards the RG. Moreover, a shock-front expands out of the system through the circumbinary medium.

2.2. Calculation of the spectra

Composite models considering both photoionization and shocks in a consistent way were adopted (Contini 1997 - Angeloni et al. 2010).

In the past years we carried out the analysis of SSs (WD + RG + nebulae + dusty shells) of both line and continuum spectra emitted from the nebulae downstream of shock-fronts and of dusty shells ejected by the RG. In particular, the observed SED was disentangled into the different components by adjusting model calculations to the data in the different frequency ranges. The models were constrained by cross checking the line ratios with the continuum. Comparison with the *absolute* observational data determines the radius of the nebulae throughout the SS.

The collision of the outburst high velocity ejecta with the RG wind and/or with the ISM surrounding the WD on the side opposite the RG (Contini et al. 2009a), induces the high temperatures downstream of the shock-fronts and, consequently, to X-ray emission (Angeloni et al. 2010, fig. 4), while in the UV domain the WD bb flux dominates. However, the data in the X-ray range were not always sufficient to distinguish the origin of the far-UV - soft X-ray emission. Both the bb tail from the WD and bremsstrahlung emitted from nebulae downstream of relatively fast shocks were proposed (e.g. Contini & Formigini 1999, fig.4).

In particular, the nebulae downstream are photoionized and heated by the flux from the WD and collisionally by the shock.

The gas entering the shock-front is compressed and heated in the post shock-region. The flux from the WD and the secondary diffuse radiation flux are calculated throughout a large number of slabs downstream (up to 300) by radiation transfer. The gas cools down by free-free, free-bound and line emission. The temperature drop is calculated smoothly downstream throughout the slabs whose geometrical thickness is automatically calculated by the temperature gradient. The computation halts when the the gas is cool enough in the radiation bound case, or, in the matter bound case, when the edge opposite to the shock-front is reached.

We use for the calculation of the spectra the code SUMA¹, which simulates the physical conditions of an emitting gaseous nebula under the joint effect of photoionization from an external source and shocks, and in which line and continuum emission from gas are calculated consistently with dust reprocessed radiation as well as with grain heating and sputtering.

3. The spectra

In AG Dra, the broad and narrow components of the line profiles reveal high (700 to 3000 km s⁻¹) and low (100-160 km s⁻¹) velocities at the epochs corresponding to the outbursts. The contemporary presence of high and low velocity shocks between the stars with a velocity gap by a factor > 10 indicates that the matter is highly fragmented by instabilities at the fluid interface (Richtmyer-Meschkov, Kelvin-Helmoltz, Rayleigh-Taylor) created by the outburst. Alternatively, the high velocities may characterize the shocks accompanying the blast wave created by the outburst in directions opposite to the RG. These shock-fronts can be treated by the dynamical evolution described by Chevalier (1982) in supernova atmospheres (Contini et al. 2009a). We will see in the following that the latter hypothesis gives a more acceptable explanation of AG Dra observations.

Following our method, first we model the line ratios, which constrain the model, then we cross check the results by comparing the calculated continuum SED with the data.

To constrain the models, the spectra should contain enough significant lines, such as those from the same element but from different ionization levels which give information about the conditions of the emitting gas independently of relative abundances, and lines from the same level of different elements which lead to different stratifications of the ions downstream, depending on the ionization potential. Comparison of line ratios in the UV and in the optical range also helps understanding the gas conditions within the SS.

The SED reveals the relative importance of the different contributions to the continuum (the radiation from the stars, the bremsstrahlung from the nebulae, and the reprocessed radiation from dust grains). Generally, in SSs, the SED shows that different nebulae contribute to the spectra. Their relative contributions must be consistently accounted for also in the calculations of the line ratios (Contini et al. 2009b) leading to an iterative

calculation process which stops when the calculated spectra and the data are well tuned.

The data are observed at Earth, while the calculations refer to the nebula. By adjusting the calculated to the observed absolute continuum by the factor $\eta \sim r^2/d^2$, which depends on the radius r of the nebula and on the distance d to Earth, some information about the location of the nebulae is obtained.

3.1. UV and optical lines

We refer to the UV and optical spectra observed by GVIG99 between June 1979 and February 1996. To get a first estimate of the conditions in the nebulae at different epochs, we combined the spectra in the UV and in the optical range observed at adjacent days. This allows to refer also the UV line ratios to H β which is one of the most significant lines. The analysis of the line ratios reveals both the physical conditions and the relative abundances of the elements throughout the nebulae. We thus selected the UV spectra at 8 epochs: 4-11-1985 (JD 2446374), 18-1-1986 (JD ..6449), 30-4-1986 (JD ..6551), 27-2-1993 (JD ..9046), 4-7-1994 (JD ..9538), 6-12-1994 (JD ..9693), 28-7-1995 (JD ..9927), and 14-2-1996 (JD 245128) which are randomly chosen phases. The selected dates are indicated upon the diagram presented in Fig. 1 (bottom), where we report the profile of the H β flux observed during the 1985-1986 and 1994-1996 active phases by GVIG99 (fig. 4, bottom diagram) and by Mikolajewska (1995).

Optical line observations are given by GVIG99 (table 2). The dates closest to the 8 epochs chosen for the UV observations are: 25-10-1985, 21-1-1986, 22-5-1986, 10-1-1993, 1-7-1994, 26-12-1994, 19-8-1995, and 3-1-1996, respectively.

The observations (GVIG99) show that the spectral region includes strong emission lines of hydrogen, helium, and weaker lines e.g. FeII and NIII. During the active phases the strongest emission lines, HeII 4686, H β and H γ , display extended wings (FWZI \leq 3000 km s⁻¹) whose intensity is generally 10% of the emission peak (GVIG99). Broad wings were observed in the HeII 1640 line during the 1981 bright phase.

The optical spectra contain the weak forbidden [OIII] 4363 line which has a relatively low critical density for collisional de-excitation ($\sim 10^5$ cm⁻³) for O²⁺. Moreover, the [OIII] 4363 line is observed even if [OIII] 5007, 4959, which are generally the strongest lines, are absent. We obtain therefore an upper limit on the density. The observed [OIII] 4363 line, although very weak, indicates a stratification of temperatures and densities of the emitting gas, in agreement with the profile of the physical conditions downstream of a shock-front.

The HeII 4686/HeI 5876 line ratio gives information about the photoionization flux and the recombination conditions of the gas.

In the UV, a strong NV 1240 depends on both the shock velocity and the intensity of the primary flux, while MgII 2800, which is a relatively strong low-level line depends indirectly on the density, which speeds up the cooling rate throughout the nebula. Actually, MgII can be strong if the emitting nebula is geometrically thick and radiation bound. The binary separation constrains the geometrical thickness of the radiative nebula, yielding a lower limit on the density downstream. The HeII

¹<http://wise-obs.tau.ac.il/~marcel/suma/index.htm>

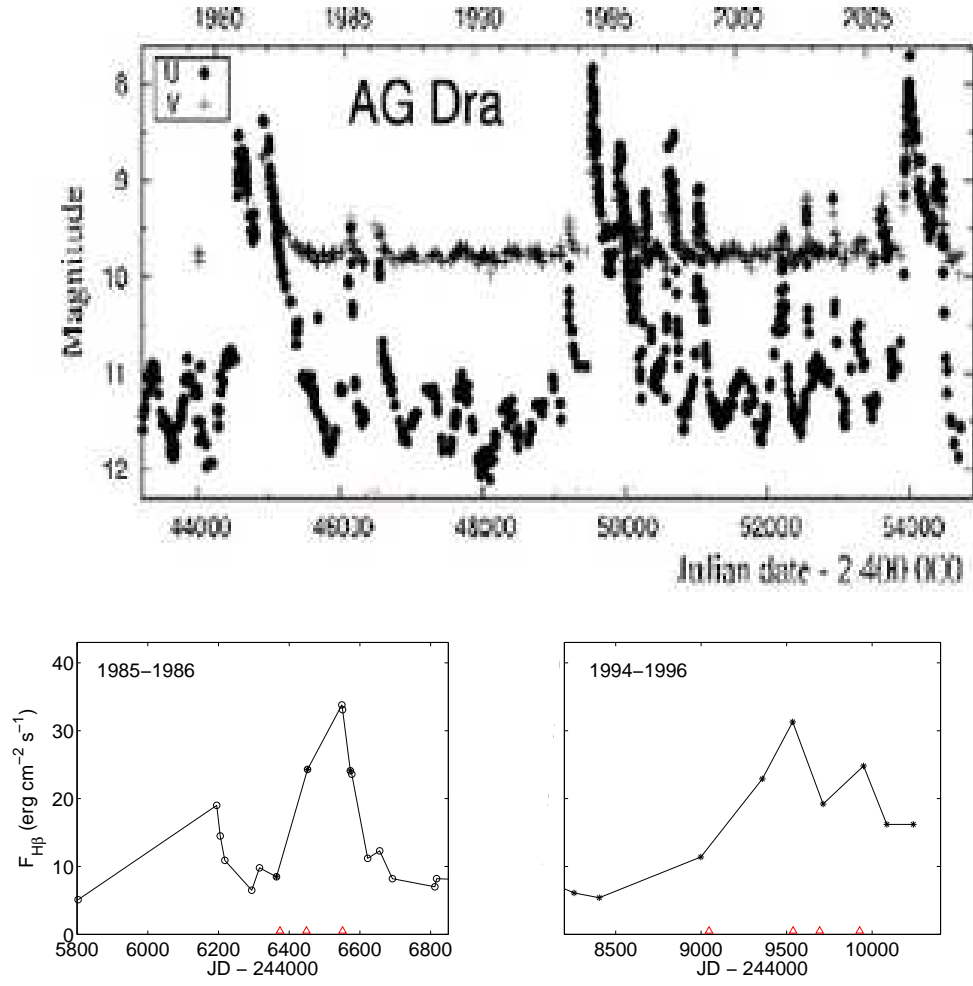


Figure 1: Top diagram: the U and V light curves of AG Dra from 1977 adapted from Skopal et al. (2009, fig.1, left diagram). Bottom diagram: variation of the strongest optical lines adapted from GVIG99, fig. 4. The red triangles indicate the JD selected for modeling (see text).

1640/OIII]1660 line ratio plays a key role in the choice of the parameters, the density in particular.

We have run a grid of models for each spectrum, first selecting the physical parameters which best reproduce the line ratios, then changing the relative abundances as a last refined improvement, particularly for CIV and MgII which are the only representative lines of C and Mg, respectively.

We reproduced the observed line ratios as close as possible considering observational errors and modeling approximation. A fit within a factor of 2 is generally accepted. However, at some epochs, the optical lines, particularly [OIII] 4363 and HeI 4471, are underestimated by the models which explain the line ratios in the UV. This indicates that the emission from the expanding nebula, which is characterized by relatively low densities, must be added. Besides stronger [OIII] and HeI lines, this nebula emits strong OI and MgII because it is extended enough to contain a region of recombined gas.

After a first rough modeling of the different spectra we have realized that the temperature of the WD is rather stable at $\sim 1.6 \times 10^5$ K on the days considered, so we iterated the modeling process adopting for all the models this temperature in agreement with Skopal et al. (2009) and Greiner et al. (1997) results by a fit to ROSAT quiescence data. Piro et al. (1985) derived a bb temperature of 200000 K from June 1985 EXOSAT observations and the Zanstra temperatures derived from the HeII/F(1340 Å) was 109000 ± 5400 K in quiescence (GVIG99).

In the phases close to outbursts, both the HeII 1640/H β and HeII 4686/H β line ratios are very high. However, HeII 1640/H β = 14.9 cannot be reproduced by the coefficients (recombination, dielectric recombination, etc.) of He and H adopted in the calculations (Osterbrock 1988 and references therein). Notice that these lines are saturated during the outbursts so it is difficult to determine the broad and narrow line relative intensity. The best fit to the line spectra is obtained by adopting a relatively high shock velocity which leads to extended regions of gas ionized to high levels. A high ionization parameter produces higher ratios to H β of intermediate ionization level lines (e.g. [OIII]/H β), while a high pre-shock density increases the cooling rate downstream changing the stratification of the ions and enhancing the low ionization level lines.

We present in Table 1 the results of modeling and we compare them with the observational data. The dates corresponding to the UV spectra are shown in column 1, followed by the observed UV and optical line ratios to H β . The observed line and continuum fluxes were reported and corrected adopting $E_{B-V}=0.05$, by GVIG99. In Table 1, next to each row containing the observed line ratios the calculated ones are shown. Models m1-m8 which provide the best fit to the data appear in the first column of Table 1. Model m_{exp} corresponds to the expanding nebula.

Models m1-m8 and m_{exp} are described in Table 2, in terms of the physical conditions in the emitting nebulae, selected as input parameters in the SUMA calculation process. They lead to the best approximation of calculated to observed line ratios. The first column of Table 2 shows the parameters which vary from epoch to epoch, while those which were found roughly constant are described in the bottom of the table. The shock

velocity V_s , the pre-shock density n_0 , and the pre-shock magnetic field B_0 refer to the shock, while the color temperature of the hot star T_* and the ionization parameter U refer to the photoionizing flux from the WD. The geometrical thickness of the emitting nebula D determines whether the model is radiation or matter bound. The dust-to-gas ratio (d/g) is crucial to explain the SED in the IR. The relative abundances to H of the elements appear in rows 6-9 of Table 2. The absolute H β flux calculated at the nebula is also given in Table 2, because it allows to calculate the absolute fluxes of all the lines. A magnetic field $B_0 = 10^{-3}$ gauss is adopted for all models.

The calculated line ratios presented in Table 1 refer to the reverse shock between the stars (Sect. 2). Therefore, the shock-front edge of the emitting nebula downstream corresponds to the edge of the nebula reached by the photoionization flux from the WD. The velocity of the reverse shock is generally considered approximately stable. A previous analysis (e.g. Contini & Formigginì 2003) concludes that the reverse shock between the stars is actually a standing shock, although disrupted by R-T and K-H instabilities.

The values of the input parameters which appear in columns 2-12 were selected because they explain the observational data. They will be considered as *results* of our modeling.

In order to understand the trend of the line ratios, we show the profile of the electron temperature T_e and electron density N_e downstream, as well as that of the most significant ions, as a function of the distance from the shock-front in Fig. 2 for the nebulae relative to models m1, m5, and m5_b (see Sect. 2.3). Recall that the density downstream is higher than the pre-shock density by a factor which depends on V_s (besides the factor of 4 determined by the adiabatic jump at the shock-front) and B_0 . The physical conditions downstream follow the recombination and cooling rates, so lines from different ionization levels are emitted from the gas at different distances from the shock-front.

The temperature of the gas is maximum in the immediate post-shock region $T \sim 1.5 \cdot 10^5$ ($(V_s/(100 \text{ km s}^{-1}))^2$), then it decreases following the cooling rate determined in each slab by free-free, free-bound and line emission rates. At a temperature $\leq 10^5$ K recombination produces strong line emission. However, the temperature is maintained at $\leq 10^4$ K by the primary radiation from the WD and the secondary radiation from hot gas slabs, collisionally heated by the shock. Low ionization and neutral lines emitted from this region weaken in geometrically thin clouds.

3.2. Broad lines

GVIG99 present the broad component flux of HeII 4686 and H β corrected for extinction in their table 2. We have constrained the model assuming V_s between 700 and 3000 km s $^{-1}$, $n_0 > 10^7$ cm $^{-3}$, U is derived from the HeII^b/H β ^b ratio, and the radius of the nebula within the AG Dra system (Sect. 4.2). We have found that $V_s = 1000$ km s $^{-1}$, $n_0 = 3 \cdot 10^7$ cm $^{-3}$, and $U = 100$ gives HeII^b/H β ^b = 1. The observed ratio is 1.6. The H β ⁿ/H β ^b line ratio, calculated by this model, results in 15.2 at Earth in agreement with GVIG99 observations. Models m2_b, m5_b, etc., are calculated adopting solar abundances because sputtering destroys the grain at such high V_s (Fig. 2).

Table 1: Comparison of calculated with observed line ratios¹ to $H\beta = 1$

	NV 1240	OI 1340	OIV]+ 1400	NIV] 1486	CIV 1550	HeII 1640	OIII] 1663	MgII 2800	HeII 3200	H γ 4340	[OIII] 4363	HeI 4471	HeII λ 4686
4/11/85	1.16	0.165	1.06	0.34	1.14	3.49	0.34	0.33	0.34	0.36	0.001	0.025	0.74
m1	0.9	0.18	0.8+	0.6	1.47	4.7	0.4	0.32	0.28	0.37	0.0014	0.026	0.65
18/1/86	2.078	0.	0.88	0.37	2.95	14.66	0.26	0.2	0.65	0.51	0.009	0.049	1.4
m2	2.56	0.	1.1	0.23	4.3	7.	0.2	0.07	0.4	0.45	0.	0.07	0.85
m2 _b	0.4	0.	0.	0.	0.2	8.9	0.	0.	0.53	0.49	0.	0.	0.1
m _{exp}	0.002	0.15	0.02	0.02	0.064	1.88	0.23	2.44	0.11	0.4	0.04	0.11	0.27
30/4/86	2.39	0.2	1.26	0.28	2.26	4.	0.253	0.0	0.33	0.44	0.006	0.045	0.64
m3	2.2	0.1	1.8	0.12	1.9	5.8	0.26	0.24	0.35	0.43	1e-4	0.01	0.78
27/2/93	0.78	0.001	0.35	-	0.58	2.97	0.175	0.184	0.44	0.35	0.001	0.036	0.526
m4	0.6	0.001	0.32	0.035	0.69	3.	0.18	0.17	0.20	0.46	0.	0.03	0.42
4/7/94	3.9	0.0	3.35	0.72	2.	10.	0.63	0.112	0.473	0.38	0.	0.093	0.86
m5	3.63	0.0	3.7	0.5	3.	6.6	0.5	0.12	0.40	0.43	4e-4	0.004	0.86
m5 _b	0.2	0.0	0.17	0.04	16.7	5.5	0.2	2.5	0.33	0.45	1.e-4	0.015	0.75
6/12/94	1.24	0.125	1.474	0.161	1.55	6.95	0.4	0.13	0.35	0.39	0.011	0.049	0.64
m6	1.1	0.01	1.6	0.35	1.53	6.	0.7	0.13	0.3	0.44	0.001	0.01	0.78
m6 _b	0.06	0.005	0.05	0.014	6.	3.7	0.11	4.6	0.22	0.46	0.	0.026	0.53
28/7/95	1.5	0.42	1.61	0.58	2.73	8.85	0.5	0.185	0.274	0.42	0.017	0.06	0.63
m7	1.88	0.	2.	1.1	2.1	7.	0.6	0.19	0.42	0.44	0.004	0.004	0.89
14/2/96	0.52	0.1	0.66	0.48	1.14	3.57	0.376	0.086	0.12	0.34	0.015	0.049	0.53
m8	0.5	0.1	0.7	0.46	1.58	4.6	0.46	0.054	0.27	0.39	0.02	0.03	0.64

¹ González-Riestra et al. (1999, Tables 1 and 2)

Table 2: Description of the models

model	m1	m2	m2 _b	m3	m4	m5	m5 _b	m6	m6 _b	m7	m7 _b	m8	m _{exp}
V _s	130	100	1000	150	100	140	700	120	700	180	700	120	100
n ₀	5.e8	2.4e10	3.e7	8.e9	3.e9	2.e9	5.e8	1.e9	5.e8	5.e7	5.e8	3.e7	3.e6
U	2.5	1	100	0.1	0.5	0.2	5	0.06	5	0.4	5	2	0.1
D	2.6e13	7.8e10	4.2e13	5.5e7	6.e11	8.8e8	4.5e11	6.e8	4.6e11	3.7e10	4.6e11	4.1e14	1.e14
H β	2.2e7	2.8e8	2.2e4	1.5e5	9.2e7	2.8e4	9.4e6	2.5e4	3.0e7	2.6e3	3.0e7	3.8e6	5.9e3
C/H	1.3e-5	8.0e-6	3.3e-4	1.3e-5	1.2e-5	1.3e-5	3.3e-4	1.7e-5	3.3e-4	1.e-5	3.3e-4	1.3e-5	1.3e-5
N/H	4.e-5	2.1e-5	9.1e-5	2.1e-5	8.1e-5	2.1e-5	9.1e-5	2.1e-5	9.1e-5	2.1e-5	9.1e-5	2.1e-5	2.1e-5
O/H	2.e-4	1.6e-4	6.6e-4	1.6e-4	1.6e-4	1.3e-4	6.6e-4	1.6e-4	6.6e-4	1.e-4	6.6e-4	1.6e-4	1.6e-4
Mg/H	2.e-5	2.e-5	3.e-5	3.e-6	2.0e-6	1.5e-5	3.e-5	3.e-6	3.e-5	4.e-5	3.e-5	3.e-6	3.e-6
r	8.4e13	2.4e13	4.2e12	7.5e14	2.6e13	9.4e14	1.8e11	1.7e15	1.88e11	1.9e15	1.3e11	1.7e14	2.4e14
R	5.8e12	1.6e12	6.7e12	3.4e12	4.8e12	5.6e12	4.e11	1.6e13	2.0e11	2.e13	5.3e11	2.8e13	2.e14
η	-15.8	-17.	-18.5	-14.	-16.9	-13.5	-21.3	-13.	-21.2	-12.9	-21.5	-15.3	-15.

V_s is in km s⁻¹, n₀ in cm⁻³, D in cm, and H β is in erg cm⁻² s⁻¹.For all the models B₀=10⁻³ gauss, T_{*}=160000 K, He/H = 0.1, Ne/H= 8.3 10⁻⁵, Si/H=3.3 10⁻⁶, S/H= 1.6 10⁻⁶, A/H = 6.3 10⁻⁶, Fe/H = 6.2 10⁻⁶, and d/g=10⁻¹⁴ by number.

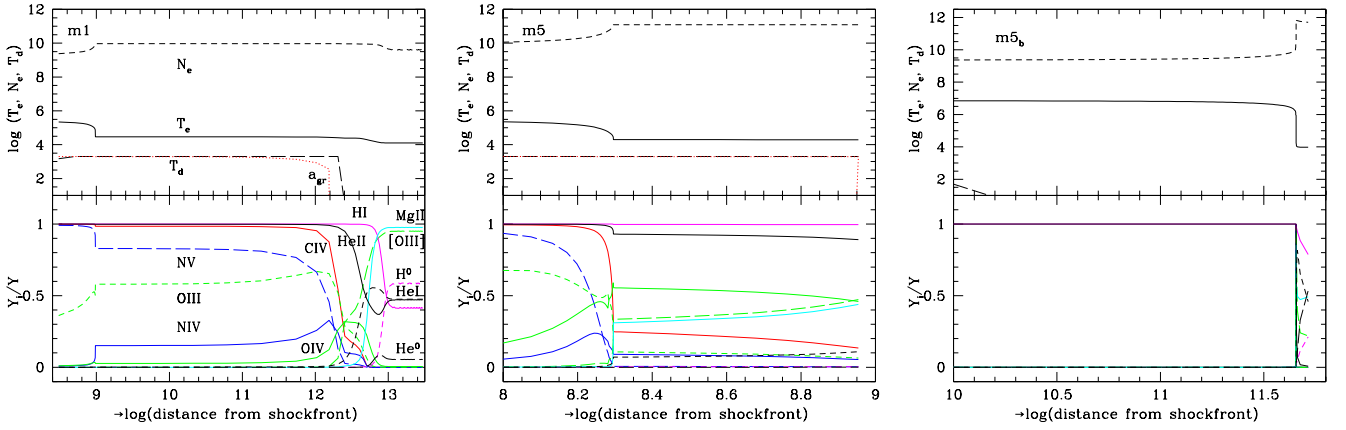


Figure 2: Top panels: the profiles of the electron temperature, electron density and the dust temperature in the regions downstream emitting the different lines for models m1 (left diagram), m5 (middle) and the model calculated with $V_s = 700 \text{ km s}^{-1}$ (right diagram). The dotted red line refers to the grain radius a_{gr} in Å. Bottom panels: the profiles of the most significant ion relative fractions.

In the following active phase, starting at day 4/7/1994, we found that a model with $V_s = 700 \text{ km s}^{-1}$, $n_0 = 5 \cdot 10^8 \text{ cm}^{-3}$ and $U = 5$ reproduces the observed $\text{He II}^b/\text{H}\beta^b \sim 0.8$ for $D = 4.55 \cdot 10^{11} \text{ cm}$ and ~ 0.5 for $D = 4.6 \cdot 10^{11} \text{ cm}$, as observed on 6/12/1994, and 28/7/95, respectively. The $\text{He II}/\text{H}\beta$ ratios in fact decrease with temperature at larger geometrical thickness. We do not have enough data to further constrain the input parameters of models m6_b and m7_b and they are therefore identical. These models contribute a weak broad component to the CIV line profile, which is not confirmed by the observations (GVIG99). Carbon could be included in small graphite grains which are, however, completely sputtered at such relatively high shock velocities. Therefore, depletion of carbon could be due to the presence of CO molecules, the second most abundant species in the ISM after H_2 .

3.3. The continuum SED

In Fig. 3 we compare the observed continuum SED with model calculations at each of the selected epochs.

The analysis of the line spectra at each epoch determines the bb temperature of the WD and the characteristics of the nebulae downstream of the network shock-fronts. The analysis of the continuum SED reveals the presence of dust shells. The temperature of the RG is approximated by a bb flux. We use an effective temperature of the cool star $T_{eff} = 4300 \text{ K}$ consistent with AG Dra's classification as an early K giant (Lutz et al. 1987).

To constrain the continuum we have used the two data observed at 1340 and 2880 Å by GVIG99. Indeed two points are too few to give a somehow complete information, however, the two wavelengths reported are strategic enough because one (2880 Å) belongs to the bremsstrahlung from the nebulae and the other (1340 Å) often to the bb flux from the WD.

The nebulae are located in the circumstellar region between the stars and/or in the circumbinary regions. The radius r of the nebulae can be obtained by comparing the calculated with the

observed absolute fluxes. They are given in the bottom of Table 2 providing a picture of the system on a large scale (Sect. 4.2).

In Fig. 3 we present the observations obtained in the X-ray and UV ranges by XMM and FUSE, respectively by Skopal et al. (2009, fig. 2, left panels). The data in the radio come from Mikolajewska (2002). We have inserted them in the spectrum referring to 30/4/1986, even if the epochs were not exactly the same, to constrain the bremsstrahlung in the radio range. Actually, Angeloni et al. (2010) claim that radio variability also throughout a relatively long period does not affect the main results of modeling. The optical low-resolution spectrum comes from the Loiano observatory and the flux points are determined by broad band optical UBVR_CLC and near-IR JHKLM photometry (Skopal et al. 2009).

4. Results

We have modeled the line and continuum spectra emitted from AG Dra at different phases at epochs corresponding to close UV and optical observation days. The results are presented in the following.

4.1. Gas physical conditions

The input parameters V_s , n_0 , and U which provide the best fit of the line ratios at different epochs are shown in Fig. 4 (left diagram).

We found low-velocity (lv) shocks with V_s between 100 and 180 km s^{-1} , in agreement with the FWHM of the UV high-level line profiles ($v = 100\text{--}160 \text{ km s}^{-1}$), e.g. MgVII 2510, 2629, SiVII 2147, etc., reported by Young et al. (2006) from recent Hubble Space Telescope STIS observations.

The high velocity (hv) shocks ($V_s = 700\text{--}1000 \text{ km s}^{-1}$) explain the broad wings in the Balmer lines observed close to the outburst epochs. They are essential in modeling the high He II 1640/H β line ratios at the dates 18/1/1986, 4/7/1994, and 28/7/1995. The hv shocks accompany the blast wave from the explosion, which propagates radially, except towards the RG,

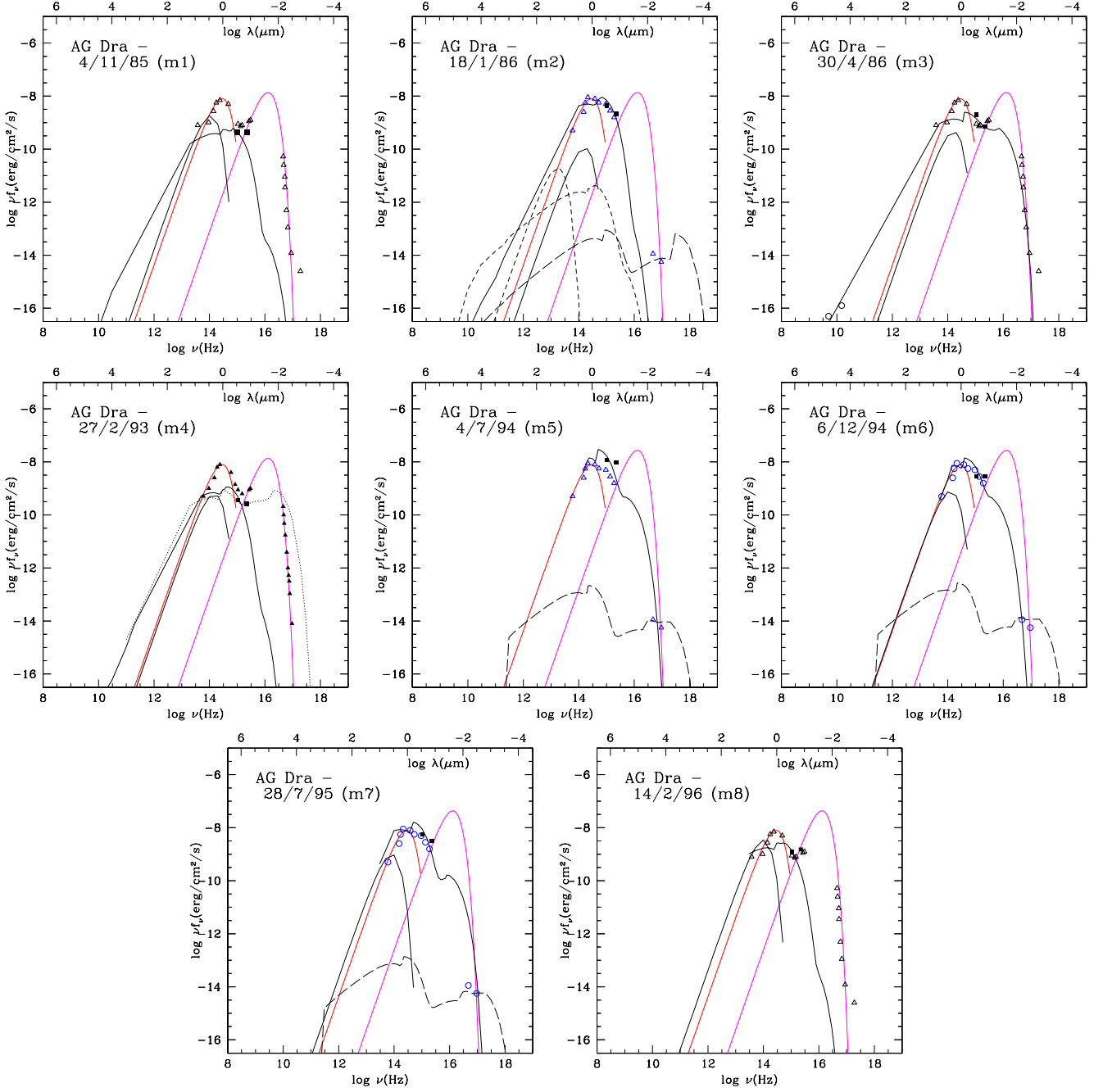


Figure 3: The modeling at different phases. The observations by Skopal et al (2009) are indicated by triangles: open blue at burst, filled black at quiescence, open black at transition. Black filled squares are the continuum data from GVIG99. Red solid line: the bb flux from the RG; solid magenta line: the bb flux from the WD; solid black line: the two curves represent the bremsstrahlung from the nebulae described in Table 2 and reprocessed radiation by dust; long-dashed black line: the bremsstrahlung from the high velocity models; short-dashed black line: the expanding nebula; dotted line: bremsstrahlung from a model calculated by $V_s = 280 \text{ km s}^{-1}$.

where collision with the dense RG wind prevents its expansion and creates a complex network of shock-fronts.

The SEDs of the continuum emitted from the nebulae downstream of the hv shock-fronts are very different from those reported by Skopal et al. in quiescent and transition phases (Fig. 3). In particular they produce negligibly low UV-optical fluxes. On the other hand the continuum SEDs emitted from the nebulae downstream of the lv shock-fronts between the stars can reproduce the trend of the observations in the soft X-ray range for $V_s \geq 150 \text{ km s}^{-1}$. For $V_s > 180 \text{ km s}^{-1}$ the X-rays can even overcome the bb flux from the WD, mimicking a higher WD temperature. For example, the SED calculated with $V_s = 280 \text{ km s}^{-1}$ in the transition phase on 27/2/1993 is shown in Fig. 3.

The pre-shock densities are relatively high, leading to the low velocities accompanying the reverse shock between the stars in AG Dra (from conservation of mass at the shock-front: $n_0 v_0 = n_1 v_1$, where 0 refers to upstream and 1 to downstream conditions). In R Aqr the velocities of the reverse shock are $\sim 100 \text{ km s}^{-1}$ and the densities are $\sim 10^5 \text{ cm}^{-3}$ (Contini & Formiggini 2003). The velocities of the reverse shock inferred from the IR line ratios in D-type SS (Angeloni et al. 2007a) are $\sim 400\text{-}500 \text{ km s}^{-1}$. We wonder whether dust and/or higher densities could be responsible for the deceleration of the reverse shock.

The input parameter U varies between a maximum of 100 in the high velocity nebulae to a minimum of 0.06 for model m6. A high U indicates that the nebula is close to the hot source and/or that there is no matter obstructing the photoionizing flux (cfr. for Z And - Contini et al. 2010, in preparation).

4.2. Radius of the nebulae

The comparison of the continuum fluxes calculated at the nebula with those observed at Earth determines the radius r of the nebula by the factor η ($r^2 = 10^{-\eta} d^2 ff$, where ff is the filling factor, d the distance to Earth of AG Dra). Adopting $d = 2.5 \text{ Kpc}$ (GVIG99) and $ff = 1$ we obtain the radius upper limits which appear in row 10 of Table 2. Considering that the binary separation is $2.3 \cdot 10^{13} \text{ cm}$ (Leibowitz et al. 1985, Tomov & Tomova 2002) ff is likely to be $\sim 0.1\text{-}0.01$.

We have calculated the distance of the inner edge of the nebulae from the WD by combining F (the number of photons $\text{cm}^{-2} \text{ s}^{-1}$ reaching the nebula) with the ionization parameter U calculated phenomenologically by modeling the line spectra, $F (r_{WD}/R)^2 = U n c$, where r_{WD} is the radius of the WD ($0.08 R_\odot$ GVIG99), n the density and c the speed of light. The resulting R are given in row 11 of Table 2.

Model (m_{exp}) should be added to the reverse shock models at the dates 30/4/1986, 4/7/1994/, and 28/7/1996, increasing the flux of the low-ionization and neutral lines. This model represents the nebula downstream of the shock propagating out of the system (Contini et al. 2009c). The shock-front edge of the nebula is opposite the edge reached by the flux from the WD. n_0 is lower and the nebula is extended. On the other hand, the

nebulae downstream of the hv shocks ($700\text{-}1000 \text{ km s}^{-1}$) have a very small radius because they represent matter ejected at the outburst which had not yet the time to propagate in the surroundings of the WD.

4.3. Integrated UV and soft X-ray fluxes from the nebulae

The input parameters (Fig. 4 left) explain the trend of the integrated fluxes (Fig. 4 right) in the optical F_{opt} (8267-3100 Å), UV F_{UV} (3100-620 Å), and in the soft X-ray range F_X (0.1-1.2 keV). The maximum gas densities downstream, i.e. the densities which are used to calculate the fluxes for each model are shown in the right diagram, as well as the E.M. (the emission measure $\Sigma D n n_e$). It can be noticed that F_{opt} and F_{UV} follow the trend of U , while F_X increases with V_s , because the maximum temperature downstream is $\propto V_s^2$.

A rough anti-correlation (Fig. 5) is evident between F_X and F_{UV} calculated at the nebula by models m1 - m8, m2_b, and m5_b. The fluxes calculated in models m6_b and m7_b coincide with m5_b, therefore, they are removed from Fig. 5 for the sake of clarity. Recall that the higher V_s the larger is the high temperature zone within the nebula because recombination coefficients are low. The cooling rate increases rapidly when the temperature of the nebula decreases below 10^5 K . At this stage a strong compression followed by a rapid cooling rate ($\propto n^2$) reduces the geometrical thickness of the UV emitting region (Fig. 2, diagram on the right) and the UV flux is relatively low. So the SED of the continuum from hv and lv shocks are different. In the soft X-ray range the flux from lv shocked nebulae dominates over the WD bb only for $V_s \geq 150 \text{ km s}^{-1}$.

The comparison of the fluxes calculated at the nebula with the continuum SED observed at Earth indicates that hv shocks have a radius smaller than that of lv ones (Table 2, last row), so the fluxes observed at Earth of hv nebulae would be lower by several orders of magnitude than those corresponding to lv nebulae and WD bb radiation. However, both the latter fluxes are absorbed by the envelop of debris accompanying the explosion. The drop in the X-ray counts at the outbursts can thus be explained by the different origin of the X-ray.

Summarizing, at outbursts, the X-rays are emitted from the shock accompanying the blast wave (which absorbs the WD bb flux). The observed flux is relatively low because it is diluted by the small η factor. In the quiescent and transition phases the soft X-ray data (observed at similar phases but at different epochs by Skopal et al) are reproduced by the WD bb with a contribution from the bremsstrahlung which dominates for shock velocities $\geq 150 \text{ km s}^{-1}$. The optical-UV flux is bremsstrahlung emitted from downstream nebulae photoionized by the WD bb flux.

4.4. Relative abundances

The abundances of the heavy elements relative to H which explain the observed line ratios are given in Table 2 (rows 6-9). We could model only the elements corresponding to observed lines.

The results show a strong under-abundance of the heavy elements relative to the solar ones ($C/H = 3.3 \cdot 10^{-4}$, $N/H = 9.1 \cdot 10^{-5}$, $O/H = 6.6 \cdot 10^{-4}$, $Mg/H = 2.6 \cdot 10^{-5}$, Nussbaumer et al. 1988).

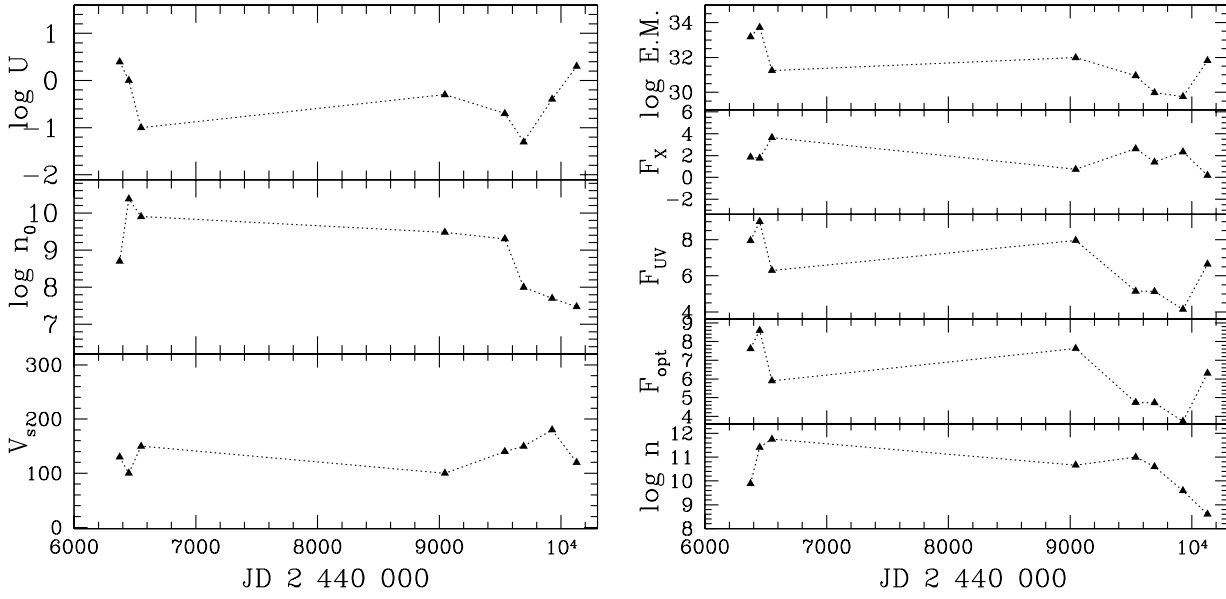


Figure 4: The input parameters (left diagram), the post-shock density, the fluxes in the optical, UV, and X-ray domain, and E.M., calculated by the models (right diagram)

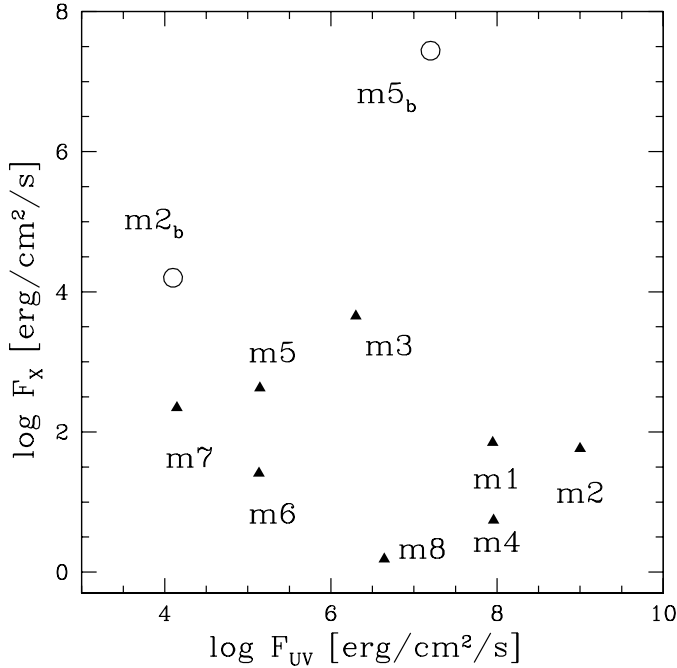


Figure 5: F_x versus F_{UB} calculated at the nebula by models which explain the line and continuum spectra. Filled triangles: low-velocity models; open circles: high-velocity models.

Nussbaumer et al. (1988) compared the O/N and C/N ratios for different objects, e.g. symbiotic stars, planetary nebulae, novae, etc. Our results show that AG Dra has C/N comparable with other symbiotic stars, but higher O/N. Moreover O/N ratios are even outside the ranges covered by the other objects.

We find C/O varying from 0.05 to 0.13, while the solar abundance ratio is 0.5. The N/H ratio is underpredicted by a factor of 4 relative to the solar, while C/H is lower than solar by a factor > 10 . Also O/H is lower than the solar by a factor of ~ 2.7 in average, while Mg/H varies between solar and 0.1 solar depending on the phase. Mg can be trapped into silicate grains, so the different abundance ratios indicate an inhomogeneous distribution of dust. We cannot comment about the Si/H relative abundance, because no Si lines are given in the spectra. SiIV] line is blended with OIV] in the 1400 Å multiplet. The calculated spectra show that the intensity of the SiIV] line is always lower than that of OIV] or similar in the case of model m4. For m4 N/H is rather solar, while C and O are depleted strengthening the hypothesis that C and O are trapped into CO molecules.

The origin of the high depletion of C, N, and O relatively to H and He is most probably due to inclusion in dust grains and/or molecules (Angeloni et al. 2007a). Dust grains are coupled to the gas by the magnetic field downstream of shock-fronts. They are heated by radiation from the WD and collisionally by the gas. Starting by an average grain radius $a_{gr}=0.2 \mu m$, Fig. 2 (top panels) shows that the grains reach a temperature < 2000 K and survive sputtering and evaporation (which are calculated consistently with the temperature of the gas) in the transition and quiescence phases, but are completely destroyed downstream of high velocity shocks.

Fig 3 shows that dust reprocessed radiation is hidden throughout the SED by the bb flux from the RG. Adopting d/g ratios (Table 2) similar to those of the ISM ($4.1 \cdot 10^{-4}$ by mass

which corresponds to 10^{-14} by number) dust emission does not contribute to the continuum sensibly. At the dates 6/12/1994 and 28/7/1995 a $d/g \sim 10^{-15}$ has been adopted. However, these results are based on the ISO observations at date 29/July/1996. Actually, dust emission can vary with phase, as was found for e.g. RS Ophiuci by Rushton et al. (2010).

Oxygen is depleted because it is trapped in unsputtered silicate grains and in CO molecules, while carbon is much more depleted (by a factor of 3) because it is trapped into graphite grains, PAHs, and diatomic molecules like CO, CN, CS, etc. (Contini & Shaviv 1982). Formation of dust species downstream of shocks is characteristic of the RG. Actually, *shock-excited* far-IR emission of CO was detected by Reach & Rho (1998) with the ISO Long-Wavelength Spectrometer from the SN remnant 3C 391.

As a result, the depletion of C, N, O and the ~ 1 year fluctuation period observed during the high outbursts in the U band and in the V band strengthens the hypothesis that this short period depends on the sudden disturbance of the dynamical field between the stars by the collision of the dusty shells ejected from the RG with the wind from the WD.

5. Discussion and concluding remarks

In previous sections we have demonstrated that the bremsstrahlung emitted downstream of shocked nebulae in AG Dra SS contributes to the soft X-rays at different phases.

GVIG99 report that after the quiescence period from 1969 to 1980 and the active phase from November 1980 and beginning 1983, a new minor outburst took place in March 1985 followed by another one after 340 days in January 1986. After 1986 a 8 years period of quiescence followed until the major active phase started in June 1994 with at least five peaks in June 1994, June 1995, July 1996, and June 1997, and one in summer 1998. They are separated by nearly the same time interval of about 360 days. Another small light maximum is present 330 days before the first maximum (Fig. 1, top).

We have reproduced the UV-optical spectra at different epochs by model calculations (Tables 1 and 2): Nov 4 1985 (m1), Jan 18 1986 (m2), Apr 30 1986 (m3), Feb 27 1993 (m4), Jul 4 1994 (m5), Dec 6 1994 (m6), Jul 28 1995 (m7), and Feb 14 1986 (m8). The bremsstrahlung calculated by model m1 refers to a transient phase, m2 to a maximum, m3 to the end of the maximum, near quiescence, m4 to quiescence, m5 is close to maximum, m6 corresponds to a transient phase in terms of a small depression between two maxima, m7 is close to maximum, and m8 represents a quiescence phase.

The classification in quiescence, maximum, and transient phases by Skopal et al. provides only a schematic picture of the physical conditions. We believe that the conditions change from burst to burst, from quiescence to quiescence, etc., because collision of the fast wind from the WD with the RG wind between the stars and with the medium inhomogeneities on the side opposite the RG, at outbursts, leads to a network of shock-fronts which varies from time to time.

Accepting that Skopal et al. (2009, fig. 2) continuum data can be applied at different epochs, Fig. 3 shows that the soft

X-rays would correspond to the bb flux from the WD in transient and quiescence epochs for shocks with $V_s < 150 \text{ km s}^{-1}$. During the 18/1/1986 burst the X-rays originated from the high velocity shock and could be observed also beyond 1 keV. After the burst, on 30/4/1986, the soft X-rays corresponding to the bb flux are comparable with the bremsstrahlung downstream of the reverse shock with $V_s = 150 \text{ km s}^{-1}$.

During the 4/7/1994 and 28/7/1995 bursts the bremsstrahlung downstream of the reverse shock corresponds to the soft X-ray range, while downstream of the blast wave shock it covers also the X-ray range ($> 1 \text{ keV}$). There are no contemporary data which could confirm our prediction in the X-ray range.

The fluctuations in the U band during the active phases between 1995 and 1999 show a ~ 360 days periodicity (Fig. 1, top diagram) which is similar to the red giant pulsation period (~ 1 year). Pulsations provoke dusty shells ejection. Collisions of the shells with the WD wind give origin to the sequence of peaks during the active phases. This is connected to the gas and dust composition in shocked nebulae. Calculation results show a depletion of C by a factor > 10 , a depletion of O by a factor of 2.7 and of N by a factor of ~ 4 , while Mg is more variable. The depleted elements are trapped into dust grains (silicates and graphite) and/or into diatomic molecules (CO, CN, CS, etc.).

The prerogative of observing the effect of the RG pulses throughout the light curve in U belongs mainly to systems which are seen nearly face-on, like AG Dra. Most information is lost in edge-on systems due to eclipses not only by the two main stars, but also by the different nebulae and shells (e.g. CH Cyg, Contini et al. 2009c) within the system.

Fig. 3 diagrams show that the continuum in the optical-UV range is emitted by the shocked nebulae between the stars. The low-frequency tail of the WD bb flux is seen at $\nu > 10^{15} \text{ Hz}$.

It was concluded by Skopal et al. (2009) that the super soft X-ray bump represents directly the WD bb flux. The peak of the WD bb between $\sim 3 \cdot 10^{15}$ and $3 \cdot 10^{16} \text{ Hz}$ is not reproduced by shock dominated models. Actually, it was neither confirmed by the observations due to the strong absorption in this range. Moreover, the H column density $N_H \sim 3 \cdot 10^{20} \text{ cm}^{-2}$ adopted by Skopal et al. (2009) to correct the data to fit the Planck function, can sensibly vary with time in a complex system such as a symbiotic one, if column densities from the emitting nebulae are accounted for.

The anti-correlation between the X-ray and UV fluxes, particularly at outbursts, was explained by the obscuration of the WD by the envelop of matter ejected at outburst which absorbs the soft X-ray emission (Skopal et al. 2009). We suggest that the absorbing envelop corresponds to the fragmented nebula downstream of the high velocity shock accompanying the blast wave, which was successfully invoked to explain some SS features, such as the broad $\text{Ly}\alpha$ line in CH Cyg (Contini et al. 2009a). The fast debris emit the broad line spectra (Sect. 3.2) and the X-ray bremsstrahlung observed at outbursts.

Finally, the results presented for AG Dra are in agreement with Smith et al. (1996) who claim by simple arguments based on the luminosity function of solar and low-metallicity K giants that yellow symbiotic stars arise among low-metallicity stars, because low-metallicity K giants have a larger mass loss rate,

thus triggering symbiotic-like activity in a binary system. Generally yellow SS show IR emission from dust (e.g. HD 330036, Angeloni et al. 2007b) which cannot be observed in AG Dra because it is hidden the bb RG flux throughout the SED. However, we have found that dust is present between the stars with a non-negligible dust-to-gas ratio ($\leq 4 \cdot 10^{-4}$ by mass).

Acknowledgments

We are grateful to the anonymous referee for his comments which improved the presentation of the paper. We thank Dina Prialnik and Elia Leibowitz for interesting conversations and Sharon Sadeh for helpful advise. RA acknowledges a grant from the FONDECYT Project N. 3100029.

References

- [1] Angeloni, R., Contini, M., Ciroi, S., Rafanelli, P. 2007a, AJ, 134, 205
- [2] Angeloni, R., Contini, M., Ciroi, S., Rafanelli, P. 2007b, A&A, 472, 497
- [3] Angeloni, R., Contini, M., Ciroi, S., Rafanelli, P. 2010, MNRAS, 402, 207
- [4] Chevalier, R.A., 1982, ApJ, 259, L85
- [5] Conti, P. S. 1978, ARA&A, 16, 371
- [6] Contini, M. 1997, ApJ, 483, 887
- [7] Contini, M., Shaviv, G. 1982, ApSS, 85, 203
- [8] Contini, M., Formiggin, L. 1999, ApJ, 517, 925
- [9] Contini, M., Formiggin, L. 2003, MNRAS, 339, 148
- [10] Contini, M., Angeloni, R., Rafanelli, P. 2009a, A&A, 496, 759
- [11] Contini, M., Angeloni, R., Rafanelli, P. 2009b, MNRAS, 396, 807
- [12] Contini, M., Angeloni, R., Rafanelli, P. 2009c, AN, 330, 816
- [13] Fekel, F.C., Hinkle, K.H., Joyce, R.R., Strutskie, M. 2000, AJ, 120, 3255
- [14] Girard, T., Willson, L.A., 1987, A&A, 183, 247
- [15] González-Riestra, R., Viotti, R., Iijima, T., Greiner, J. 1999, A&A, 347, 478
- [16] Greiner, J., Bickert, K., Luthardt, R., Viotti, R., Altamore, A., González-Riestra, J., Stencel, R.E. 1997, A&A, 322, 576
- [17] Jansen, F., Lumb, D., Altieri, B., et al. 2001, A&A, 365, L1
- [18] Kwok, S., Leahy, D.A. 1984, ApJ, 283, 675
- [19] Leibowitz, E.M., Formiggin, L., Netzer, H. 1985, ESASP.236, 109L
- [20] Lutz, J.H., Lutz, T.E., Dull, J.D., Kolb, D.D. 1987, AJ, 94, 463
- [21] Mikolajewska, J., Kenyon, S.J., Mikolajewski, M., Garcia, M.R., Polidan, R.S. 1995, AJ, 109, 1289
- [22] Mikolajewska, J. 2002, MNRAS, 338, L33
- [23] Mürset, U., Schmid, 1999, A&AS, 137, 473
- [24] Nussbaumer, H., Schild, H., Schmid, H.M., Vogel, M. 1988, A&A, 198, 179
- [25] Nussbaumer, H. 2000, ASP Conf. Ser. 204: Thermal and Ionization Aspects of Flows from Hot Stars, 204, 317
- [26] Osterbrock, D.E. 1988 in 'Astrophysics of gaseous nebulae and active galactic nuclei', University Science Books
- [27] Paczynski, B., Zytow, A. 1978, ApJ, 222, 604
- [28] [Piro et al.(1985)]1985IAUC.4082....3P Piro, L., Cassatella, A., Spinoglio, L., Viotti, R., & Altamore, A. 1985, IAUC, 4082, 3
- [29] Reach, W.T., Rho, J. 1998, ApJ, 507, L93
- [30] Rushton, M.T. et al. 2010, MNRAS, 401, 99
- [31] Schmid, H. M., Schild, H. 1997, A&A, 321, 791
- [32] Skopal, A., Sekeras, M., González-Riestra, R., Viotti 2009, A&A, 507, 153
- [33] Smith, V.V., Cunha, K., Jorissen, A., Boffin, H.M.J. 1996, A&A, 315, 179
- [34] Tomov, S., Tomova, M. 2002, A&A, 388, 202
- [35] Viotti, R., Greiner, J., González-Riestra, R. 1998, Nuclear Physics B (Proc. Suppl)69/1-3, 40
- [36] Young, P.R., Dupree, A.K., Espey, B.R., Kenyon, S.J. 2006, ApJ, 650, 1091